journal

J. Am. Ceram. Soc., 99 [10] 3226–3232 (2016)
DOI: 10.1111/jace.14178

Analysis of the Power Density at the Onset of Flash Sintering

Rishi Raj†

Department of Mechanical Engineering, University of Colorado at Boulder, Boulder Colorado 80309-0427

The large bank of data for ceramics from experiments in flash sintering reveal a surprising characteristic: that the transition to a highly nonlinear rise in electrical conductivity—a signature event for the onset of the flash—occurs within a narrow range of power density. This condition holds for ceramics that are semiconductors, ionic conductors, electronic conductors, and insulators.They flash at temperatures that range from 300°C to 1300°C, and at electric fields from 10 V/cm to over 1000 V/cm. Yet, the power expenditure at the transition for all of them still falls within this narrow range. This, rather uniform value of power dissipation suggests that Joule heating is a key factor in instigating the flash. A general formulation is developed to test if indeed Joule heating alone can lead to the progression of such nonlinear behavior. It is concluded that Joule heating is a necessary but not a sufficient condition for flash sintering.

I. Introduction

The onset of the abrupt increase in conductivity is the singular event in a flash sintering experiment. The question arises if this abrupt transition in conductivity is from Joule heating that springs from the Arrhenius increase in conductivity of the ceramic with temperature, or whether it is the manifestation of a new state such as an insulator to metal transition. The objective of this article is to ask whether or not the Arrhenius argument, on its own, can explain this highly nonlinear phenomenon.

The nonlinear transition occurs only if the electric field is above a critical value. For example, in the case of 3 mol% yttria-stabilized zirconia (3YSZ), as seen in Fig. 1,[1] the flash occurs when the field is ≥60 V/cm. Note that power dissipation alone cannot explain the nonlinearity; at 40 V/cm, the power dissipation is the same as at higher fields, yet the flash is absent. However, at high fields, it is striking that the onset of the nonlinearity occurs at approximately the same power density regardless of the electric field, which points to the importance of Joule heating. These data immediately suggest that Joule heating is important, but it may not be the only criterion for the flash event.

Many different oxides have been evaluated for their flash sintering behavior in our laboratory. Flash sintering occurs in $CoMnO_4$[2] which is a semiconductor, in yttria-stabilized zirconia,[3,4] an ionic conductor, in titania,[5] which is an electronic conductor, and in strontium titanate,[6] MgO-doped alumina,[7] and undoped yttria,[8] which are commonly thought of as wide band-gap insulators, complex oxides such as $BaTiO_3$,[9] and silicon carbide.[10] The case of undoped yttria is particularly interesting since it is difficult to sinter, conventionally, even above 1800°C, but can be flash sintered in mere seconds at about 1300°C. On the other hand, undoped alumina, which does sinter in the conventional way, cannot be flash sintered; indeed, it is the only oxide that we have not been able to flash within the limits of the temperature and power supplies available to us. This behavior is not compatible with temperature alone being the explanation for distinguishing conventional and flash sintering.

The temperatures for the onset of the flash in these different ceramics can vary from 300°C to 1300°C, and the field from 10 V/cm to more than 1000 V/cm. Despite the wide range of conditions, we have discovered that the onset of the nonlinearity always occurs within a narrow range of power expended in the specimen, about 10–50 mW/mm^3, as shown in Fig. 2. The "universality" of this transition is intriguing. That the transition occurs in a narrow range of power dissipation suggests that Joule heating plays a critical role. The question is if it can, by itself, explain the full progression of the nonlinearity.

II. Experimental Parameters for the Flash Transition

We analyze the Joule heating behavior with three experimentally measured parameters (i) the temperature for the onset the linearity, (ii) the power dissipation at the onset, and (iii) the activation energy for the Arrhenius rise in conductivity prior to the onset of the instability.

In this section, the data that will be used in the analysis are summarized. The results for yttria-stabilized zirconia, and MgO-doped alumina, and composites of alumina and zirconia,[11] are shown in Fig. 3. Note the widely varying fields and temperatures for the onset of the flash. For example, in 3YSZ, the flash occurs near 950°C at 50 V/cm, but moves to about 725°C at a field of 150 V/cm.[3] Magnesia-doped alumina flashes at 1300°C at a field of 1000 V/cm.[7] The composites of *undoped* alumina and YSZ flash at fields used for single-phase YSZ, but at higher temperatures.[11] For example, at 150 V/cm, 3YSZ flashes at 725°C but the composite does so at about 1075°C. (It is curious that we have been unable to flash undoped alumina, but it sinters readily when combined with 3YSZ.)

The experiments with 3YSZ carried out at heating rates ranging from 2°C/min to 20°C/min[1] (K. Naik and V. Sglavo, unpublished work) are shown in Fig. 4. They too show that the transitions occur in the same range of power density as in Fig. 3, even though the flash temperature moves to a higher value as the heating rate is increased.[3] (The movement of sintering to a higher temperature as the heating rate is increased is also seen in conventional sintering.[12]) In all of the above experiments, the samples were in the shape of dog bones with a gage section of 20 mm (long) × 1 to 2 mm (thick) × 3.3 mm (wide).[7]

Please note that if plotted as log (current density) versus $(1/T)$ the data would have spread out vertically. Since each experiment was done at a different value of E, a higher field would have induced a higher current. *It is the power density that reveals the universal property of the flash sintering phenomenon*.

(The electric field was measured in units of V/cm, the current in mA, and the cross section of the specimen in mm^2. The

H. Chan—contributing editor

Manuscript No. 37293. Received August 2, 2015; approved January 21, 2016.
†Author to whom correspondence should be addressed. e-mail: rishi.raj@colorado.edu

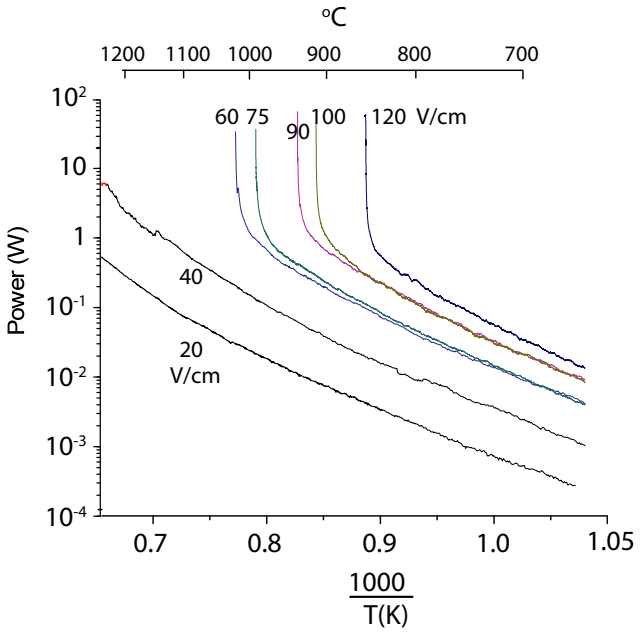

Fig. 1. The flash transition in 3YSZ plotted in the Arrhenius form of the power dissipation at different applied fields. Note that (i) the nonlinear event occurs only above a field of 60 V/cm, (ii) that the power dissipation at the point of transition remains unchanged with field, and (iii) that power dissipation on its own is not enough to pinpoint the transition since the flash does not occur at low field despite the value for power dissipation having reached the critical value which does precipitate the transition at higher fields. From Ref. [1].

power density is then calculated from the relationship $P_W(\mathrm{mW/mm^3}) = \frac{E(\mathrm{V/cm})}{10} J\left(\frac{\mathrm{mA}}{\mathrm{mm^2}}\right)$, where J is the current density. The conversion of power density from units of $\mathrm{mW/mm^3}$ to $\mathrm{W/m^3}$ is given by $P_W(\mathrm{W/m^3}) = 10^6 \times P_W(\mathrm{mW/mm^3})$.

III. The Analysis of Joule Heating

The power expended in the specimen is given by

$$P_W = E^2\sigma \tag{1}$$

where E is the applied field, and σ is the specific conductivity. We now develop a method to analyze the rise in the specimen temperature by Joule heating, where the intrinsic conductivity of the ceramic follows Arrhenius behavior. We seek to know whether or not, at a critical power density, the temperature of the specimen can rise uncontrollably.

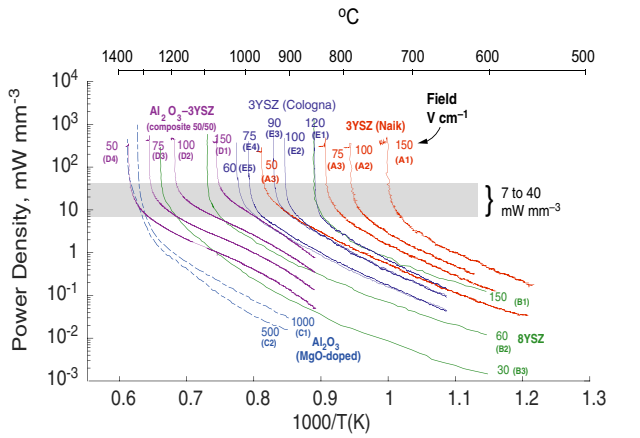

Fig. 3. Arrhenius plots of power density for several ceramics constituted from zirconia and alumina showing the transition to sudden increase in conductivity, which spells the onset of flash sintering. References are given in the text. Experiments were carried out at a heating rate of 10°C/min; the current limit was set at 80 $\mathrm{mA/mm^2}$.[11]

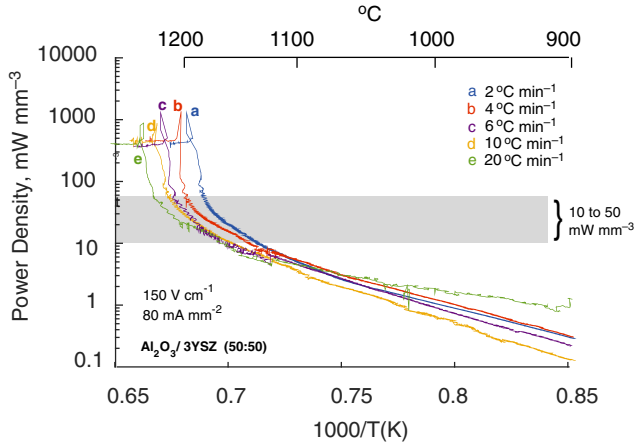

Fig. 4. Arrhenius plots of power density for 3YSZ for flash experiments with 3YSZ carried out at different heating rates.[12]

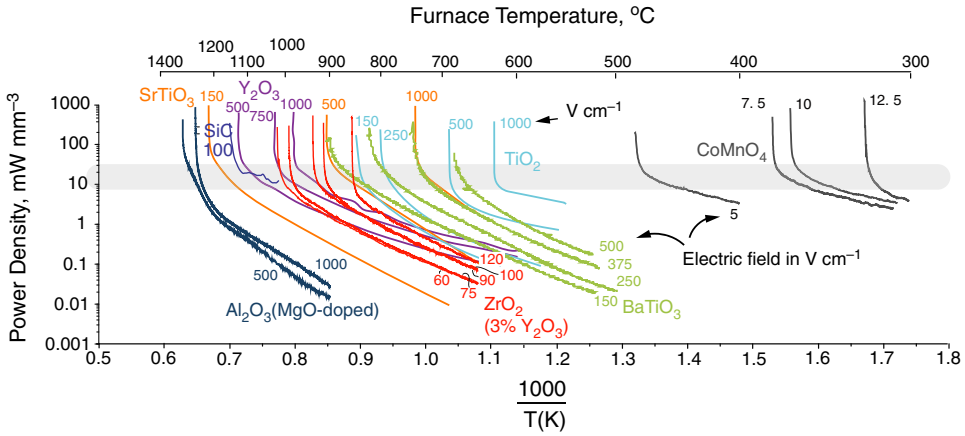

Fig. 2. The onset of flash in several ceramics in constant heating rate experiments. Note that the flash triggers at a similar power level despite the difference in their intrinsic electrical properties. References are given in the text.

An argument has been made that power dissipation, which rises exponentially with temperature, will overtake heat loss given by blackbody radiation, which increases as T^4 causing thermal runaway.[13,14] The concept proposed in these papers is indisputable: in some regime of temperature, the exponential rise will certainly rise above the power-law function. The question is whether this behavior stretches across the full horizon or whether it is limited to certain temperature regime. The analysis given here addresses this issue.

We analyze the above transition in general terms by using nondimensional parameters so that the result can be applied to many different ceramic systems in a self-consistent way.

(1) Nomenclature

V_S	m^3	Volume of the specimen
A_S	m^2	Surface area of the specimen
E	V/cm	Applied electric field
σ_{SF}	5.67×10^{-8} $W/(m^2\ K^4)$	Universal constant for black body radiation
ε_{em}		Emissivity, assumed 0.8 for oxide ceramics
P_W	W/m^3	Power density expended in the specimen
P^*_W	W/m^3	Power density at the onset of the flash transition
ρ_W	kg/m^3	Density
κ	$W\cdot(m\cdot K)^{-1}$	Thermal conductivity
$D_K = \frac{\kappa}{\rho_W C_p}$	m^2/s	Thermal diffusivity
T^*_F	Kelvin	Furnace temperature at the onset of the flash transition
T	Kelvin	Specimen temperature
$\theta = \frac{T}{T^*_F}$		The temperature is normalized with respect to the furnace temperature at the onset of the flash
$\alpha = \frac{Q}{RT^*_F}$		Normalized activation energy in the Arrhenius equation
t_d		Time constant for thermal diffusion through the specimen
$\tau = \frac{t}{t_d}$		Normalized time

(2) Analysis

The governing equation relates the rate of change of specimen temperature to the difference between the electrical power expended and the power loss by blackbody radiation. Written in units of Watts, we have

$$\rho_w C_p V_S \frac{dT}{dt} \le P_W V_S - A_S \varepsilon_{em} \sigma_{SF} (T^4 - T^{*4}_F) \quad (2)$$

Equation (2) is written as less-than-equal-to since it does not consider other modes of heat loss such as conduction and convection, in addition to blackbody radiation. Thus, the right-hand side gives the *upper bound* for the rise in specimen temperature.

In order to relate Eq. (2) to the data we write

$$P_W = P_X e^{\frac{-Q}{RT}} \quad (3)$$

which applies reasonably well up to the point of the nonlinear transition. Here, P_X is the pre-exponential. Q is the activation energy for the rate of power expenditure at constant applied voltage (it is the same as the activation energy for the Arrhenius dependence of the conductivity). The transition occurs at the power density, called P^*_W and a furnace temperature T^*_F, so that

$$P^*_W = P_X e^{-\frac{Q}{RT^*_F}} \quad (4)$$

Substituting from Eq. (4) into Eq. (3) we have

$$P_W = P^*_W e^{-\frac{Q}{R}\left(\frac{1}{T} - \frac{1}{T^*_F}\right)} \quad (5)$$

In the above equations, T represents the specimen temperature; we normalize it relative to the furnace temperature T^*_F at the transition as follows

$$\theta = \frac{T}{T^*_F} \quad (6)$$

Making this substitution in Eq. (5) gives

$$P_W = P^*_W e^{\frac{Q}{RT^*_F}\left(1 - \frac{1}{\theta}\right)} \quad (7)$$

Further writing

$$\alpha = \frac{Q}{RT^*_F} \quad (8)$$

and substituting in Eq. (7) gives

$$P_W = P^*_W e^{\alpha\left(1 - \frac{1}{\theta}\right)} \quad (9)$$

Our interest is how the specimen temperature, T, rises during this non-linearity. The rate of change with temperature is given by Eq. (2), which can now be rewritten as

$$\frac{\rho_w C_p V_S}{t_d A_S \varepsilon_{em} \sigma_{SF} T^{*3}_F} \frac{d\theta}{d\tau} \le \frac{V_S}{A_S \varepsilon_{em} \sigma_{SF} T^{*4}_F} P^*_W e^{\alpha\left(1 - \frac{1}{\theta}\right)} - (\theta^4 - 1) \quad (10)$$

where the time has been normalized with respect to the time constant for thermal diffusivity of the specimen

$$\tau = \frac{t}{t_d} \quad (11)$$

where t is the real time. The underlying argument is that the time should be normalized by the effective time for diffusing heat throughout the specimen, which is written as t_d. It is described by the relationship that (diffusion distance)^2 = $6D_K t_d$. The effective diffusion distance, ℓ, for a long cylindrical sample with the field applied to its end faces, would be equal to the radius of the cylinder. For samples with a rectangular cross section, as has been the case for the dog bone samples used in the present experiments, the effective diffusion distance would be equal to one-half of the smaller dimension of the rectangular cross section of the sample. The cross section of the specimens in our experiments was 3.3 mm × 1.8 mm, therefore the diffusion distance is set equal to 0.9 mm.

The typical time for spreading heat throughout the specimen is then given by

$$t_d = \frac{\ell^2}{6D_\kappa} \quad (12)$$

Here, D_κ, the thermal diffusivity, which has units of m^2/s, is related to the thermal conductivity, κ and the specific heat, C_p,

$$D_\kappa = \frac{\kappa}{\rho_w C_p}\ \mathrm{m^2/s} \tag{13}$$

where ρ_w has units of kg/m^3, and C_p units of J·(kg·K)$^{-1}$. Therefore

$$t_d = \frac{\ell^2 \rho_w C_p}{6\kappa} \tag{14}$$

Substituting Eq. (11), (12), (13) and (14) into Eq. (10) leads to the following final result in nondimensional parameters

$$S\frac{d\theta}{d\tau} \le R^* e^{\alpha\left(1-\frac{1}{\theta}\right)} - (\theta^4 - 1) \tag{15}$$

where

$$S = \frac{6\kappa(V_S/A_S)}{\ell^2 \varepsilon_{em}\sigma_{SF} T_F^{*3}} \tag{16}$$

and,

$$R^* = \frac{(V_S/A_S)}{\varepsilon_{em}\sigma_{SF} T_F^{*4}} P_W^* \tag{17}$$

In Eq. (15) α is given by Eq. (8), and θ is equal to the specimen temperature, T, divided by T_F^*, which is the furnace temperature at the onset of the non-linearity.

Our interest is to determine whether the rate of change of the specimen temperature after the onset of the nonlinearity is positive or negative. For this purpose, we need only consider whether the right-hand side of Eq. (15) is positive or negative—positive implying a rising temperature and negative implying a cooling scenario. A negative value of the right-hand side implies that blackbody radiation loss is greater than the heat expended electrically within the specimen; this scenario is physically inadmissible, therefore the negative values of the right-hand side of Eq. (15) are forbidden.

The left-hand side of the equation, expressed in the parameter S affects the magnitude of the result on the right; it does not affect its sign. Since, at this point, we are interested only in the sign of the right-hand side, it suffices to consider the right-hand side of Eq. (15).

IV. Prediction of Heating and Cooling

The general shape of the curve for the RHS, which is fortified by comparison with experiments in the next section, is shown schematically in Fig. 5. Recall that θ is equal to the specimen temperature divided by the furnace temperature at the onset of the nonlinearity. When $\theta = 1$, the RHS of Eq. (15) is given by RHS = R^*, where R^* is prescribed in Eq. (17). However, the RHS declines when $\theta > 1$. Indeed, as θ increases, the RHS becomes equal to zero at which point thermal equilibrium between Joule heating and BBR is achieved. Negative values of the RHS are forbidden.

Continuing to plot the RHS shows that the curve goes through a minimum, and begins to rise again, eventually entering positive territory at higher values of θ. However, it is not possible for the specimen to return to the positive regime since the negative regime is not permitted.

The form of Eq. (15) simplifies comparison with experiments. The data provide the following information, (i) the furnace temperature, T_F^*, at the onset of the nonlinearity, (ii) the power expenditure in the specimen P_W^* at the point of the nonlinear transition, and (iii) the activation energy, Q, for power dissipation leading up to the onset of the instability in the Arrhenius plot. The above three values lead to the determination of α from Eq. (8) and R^* from Eq. (17). They can now be substituted into the right-hand side of Eq. (15) to determine the change in the specimen temperature.

The values for the above parameters are given in Table I. In summary, Series A, and E refer to experiments on 3YSZ.[5,11] Series B refers to data for 8YSZ.[6] Series C refers to flash sintering experiments with MgO-doped alumina,[9] and Series D to composites of alumina and zirconia.[11] The volume to surface ratio for these specimens was 0.7 mm, which is also quoted in Table I.

We are now ready to plot the RHS of Eq. (15) for these experiments. The results are grouped into three figures. Figure 6 relates to the two sets of data for 3YSZ, and one data set for 8YSZ. Figure 7 shows the plots for MgO-doped alumina, and for the composites of alumina and zirconia. The last, Fig. 8 gives the results for the different heating rate experiments on 3YSZ. The plots start at $\theta = 1$, when the specimen temperature is equal to the furnace temperature at the onset of the nonlinear transition.

All three figures show similar trends. In few cases, the minimum for the RHS can lie above the zero line. But, more commonly, the minimum drops into the negative values which would prohibit thermal runaway on the basis of Joule heating. Indeed, we see robust flash sintering even when the curves drop into the negative regime.

Let us consider the factors that can cause some of the curves to lie above the zero line. By inspection, we note a correlation between the magnitude of the intercept on the y-axis, and the likelihood of the curve remaining in the positive regime. The value of this intercept is equal to R^*, which is given by Eq. (17). Since R^* is inversely related to the furnace temperature at the onset of the instability, specimens that flash at a lower temperature are more likely to show curves that have their minimums in the positive regime. Accordingly, the 3YSZ specimens, which were flashed with higher fields, and therefore at lower furnace temperatures, show this behavior. The relationship becomes more obvious in Fig. 7, where the data for MgO-doped alumina when the flash temperatures are high, the curves drop quickly into the negative regime. The results for alumina–

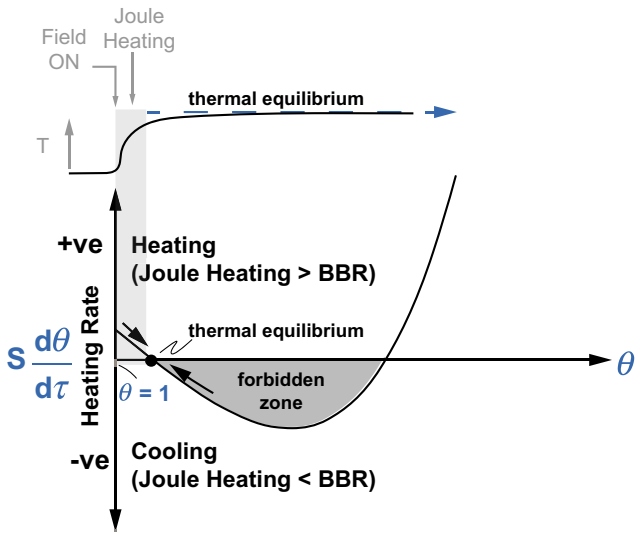

Fig. 5. A schematic of the prediction from Eq. (15). The heating rate is positive when the field is applied, but declines as the temperature rises, settling down to a steady state of thermal equilibrium between the electrical power dissipation and the heat loss from blackbody radiation. The specimen cannot cool below this temperature since blackbody radiation cannot exceed the power dissipated electrically in the specimen.

Table I. Data for Plots in Figs 6–8

Ceramics	Figs 4–6	T_F^* (K)	P_W^* (mw/mm^3)	Q (kJ/mol)	V_S/A_S (mm)	α NonDimensional	R^* NonDimensional
3YSZ[11]	A1	716	10	134	0.7	16.3	0.161
	A2	772	10	134	0.7	15.4	0.130
	A3	812	10	134	0.7	14.8	0.111
	A4	942	20	134	0.7	13.3	0.142
8YSZ[6]	B1	832	7	122	0.7	13.3	0.073
	B2	1060	7	122	0.7	11.0	0.034
	B3	1185	7	214	0.7	17.7	0.024
MgO-doped Alumina[9]	C1	1265	3	170	0.7	13.3	0.008
	C2	1287	3	191	0.7	14.7	0.008
Composites of alumina and 3YSZ[11]	D1	1038	20	191	0.7	17.5	0.104
	D2	1163	20	153	0.7	12.8	0.073
	D3	1257	20	153	0.7	12.0	0.056
	D4	1313	10	153	0.7	11.6	0.024
3YSZ[5]	E1	840	10	157	0.7	17.0	0.100
	E2	889	10	143	0.7	14.8	0.085
	E3	906	10	160	0.7	16.3	0.080
	E4	969	10	157	0.7	15.3	0.065
	E5	986	10	141	0.7	13.5	0.061
3YSZ/Alumina composites at different heating rates[12]	a	1165	25	182	0.7	15.2	0.090
	b	1177	25	190	0.7	15.8	0.087
	c	1190	25	210	0.7	17.3	0.084
	d	1195	25	229	0.7	18.8	0.083
	e	1207	25	134	0.7	10.9	0.080

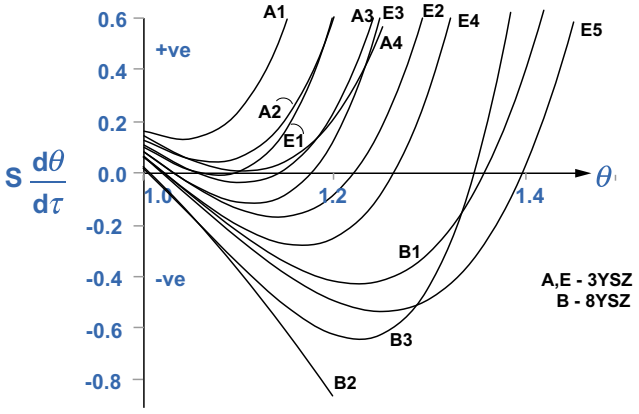

Fig. 6. Plots of Eq. (15) for the data for 3YSZ and 8YSZ as given in Table I. These data were obtained from the experimental results in Fig. 3.

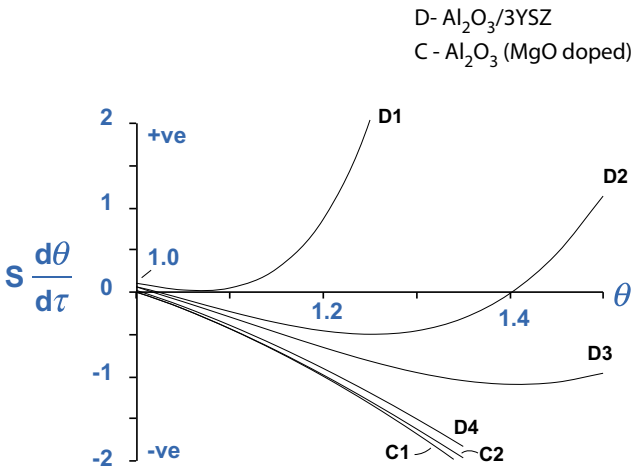

Fig. 7. Plots of Eq. (15) for the data for 3YSZ, MgO-doped alumina and composites of YSZ and undoped alumina.

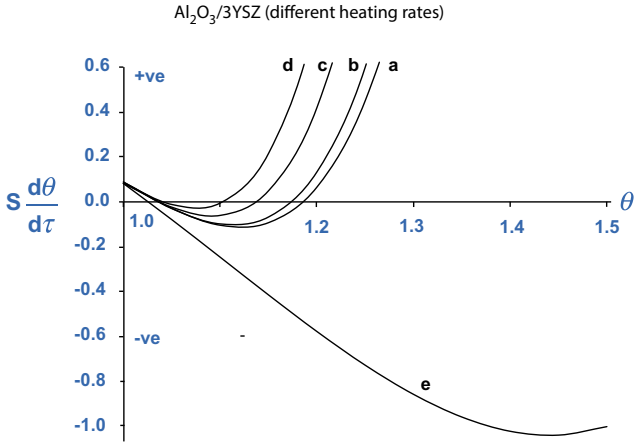

Fig. 8. Plots of Eq. (15) for the data for 3YSZ/alumina composites at different heating rates given in Fig. 4. The symbols a-e are explained in Table I.

3YSZ composites shown in Fig. 8 also have their minimums in the negative regime.

V. *In situ* Measurements of Specimen Temperature

(1) Experiments

In recent papers, we have reported results from *in situ* X-ray diffraction experiments carried out at synchrotrons where the specimen temperature is measured from thermal expansion of the lattice. Lattice expansion causes the diffraction peaks to move to a lower angle, which is translated into the change in the lattice parameter using Bragg's Law.[15,16] The peak shifts are calibrated with respect to platinum, which is incorporated into the specimen. In these experiments, the X-ray beam travels through the thickness of the specimen; therefore, the width of the diffraction peak gives a measure of the temperature gradient within the specimen (variation in temperature

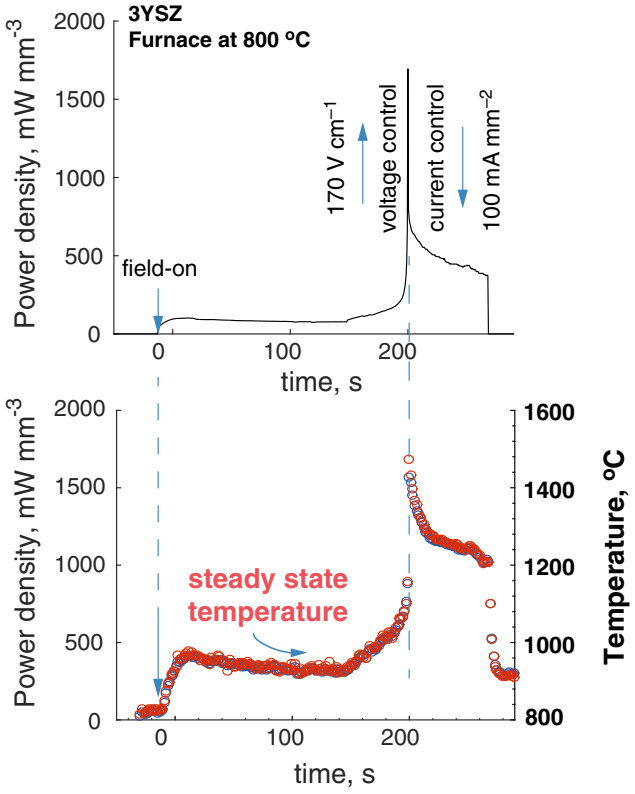

Fig. 9. Measurements of the specimen temperature from *in situ* experiments at the APS synchrotron as the field is applied as a step function. Note the specimen reaching a steady-state value, as predicted in Fig. 5. The abrupt onset of the nonlinearity after 200 s cannot be predicted from Joule heating.

would cause the intrinsic peak to move by different amounts thereby leading to broadening of the peak width).

Of interest, here is the measurement of the change in specimen temperature with time after the electric field is applied as a step function. The specimen temperature, measured as described just above, rises from Joule heating but then reaches a steady value as shown in Fig. 9, which is agreement with Fig. 5; it does not show the instability. The instability does occur but after waiting for 200 s; but, this may not be attributed to Joule heating. It is also inappropriate to argue that the delayed instability corresponds to the curve reemerging into the positive territory in Fig. 5; the temperature at which the curve turns positive lies far above the first transition when the curve crosses zero into the negative regime. It is not possible for the specimen temperature to rise from this lower value to the higher value by Joule heating alone.

It may be useful to note that in early work, where the specimen temperature was measured with a pyrometer, the temperature rose continuously through the flash transition toward a steady-state value.[17] Rigorous measurements of the specimen temperatures, from thermal expansion in real time, as reported just above, are essentially in agreement with the pyrometer measurements.

(2) Analysis of Heat Transport

It is often argued that the surface temperature of the specimen, which controls blackbody radiation, may not represent the temperature within. We have conducted *in situ* experiments to measure the specimen temperature at synchrotrons. The peak shifts are calibrated against a platinum standard without applying electric field, and the baseline peak widths are measured for specimens at a uniform temperature equal to the furnace temperature. In these experiments, the X-ray beam records the inside temperature since it travels through the thickness of the specimen before diffracting. Measurements of peak width under flash conditions are found to be unchanged from the baseline measurements, showing that the temperature gradients within the specimen, for the geometry used in our experiments, were not significant.

It is also possible to estimate the extent of the temperature gradient within the specimen by the following analysis. The gradient within the specimen must be consistent with the conduction of heat from within the specimen, where electrical power is dissipated, to its surface. The heat flux, the thermal conductivity, and the effective distance of heat flow then give the upper bound for the temperature gradient within the specimen. This analysis gives the following result

$$P_W L = \kappa \frac{\Delta T_{max}}{x_{eff}} \tag{18}$$

In Eq. (18), heat flux is expressed per unit area of the surface of the specimen. P_W is the electrical power dissipated per unit volume, L is the total thickness within which power is dissipated (it is normal to the surface of the sample where the heat is radiated to the ambient), κ is the thermal conductivity, and ΔT_{max} is the maximum temperature difference within the specimen. The effective diffusion distance for heat transport is x_{eff}. If all the power were to be expended exactly in the center line of the specimen, then x_{eff} would be equal to one-half the thickness of the specimen. However, heat is generated throughout the bulk of the specimen, therefore the effective transport distance would be much less; a conservative value would be one-quarter the thickness of the specimen, which in present experiments was 0.16 mm. Substituting $K = 2.7\ \mathrm{mW{\cdot}(mm{\cdot}K)^{-1}}$, $L = 0.65$ mm, and $P_W = 500\ \mathrm{mW/mm^3}$, we calculate that $\Delta T_{max} \approx 20°\mathrm{C}$, which is of the order of the sensitivity of the temperature gradient from *in situ* measurements as discussed just above (J.-M. Lebrun, S. K. Jha, W. M. Kriven, and R. Raj, unpublished work). In specimens with thick cross sections, greater temperature gradients can exist. However, there is little evidence to support the idea that the temperature within the specimen is very significantly different from the surface in the experiments of flash sintering carried out in the author's laboratory.

VI. Discussion

The objective of the analysis presented above was to explore whether or not Joule heating is a *necessary and sufficient* condition for flash sintering. An approach, exemplified in Eq. (15), has been developed which can be applied to the large treasure of experimental results on flash sintering of several oxide ceramics. The analysis was triggered by the observation that the transition to a nonlinear increase in conductivity, a signature of the flash event, occurs within a narrow range of power expenditure, even when the ceramics flash over a wide range of temperatures and electric fields. This observation suggests an important role for Joule heating in the flash sintering phenomenon. The question then is, as has been suggested in recent articles,[13,14] *whether or not it is also a sufficient condition for the highly nonlinear event*.

The analysis presented here has been applied to experiments carried out at a constant heating rate of 10°C/min. The analysis is suited to these experiments because they yield the activation energy for the increase in power dissipation as the furnace temperature advances toward the critical point. However, experiments have also been carried out at isothermal furnace temperatures, where the field is applied as a step function. Often, an incubation time is observed for the onset of the flash.[18] The results of the constant heating rate results would apply because at the time period of the flash lasts less

than 10 s during which the power supply is switched from voltage to current control. In constant heating rate experiments, this period corresponds to a change in furnace temperature of <5°C, that is, the transition essentially occurs under isothermal conditions.

VII. Summary

Arrhenius plots of power expenditure in specimens from the ambient to the onset of the flash in constant heating rate experiments reveal an unusual behavior. The onset of flash occurs within a narrow range of power density, even for a wide range of ceramics, which include semiconductors, electronic conductors, ionic conductors, and insulators. The flash temperature can vary from 300°C to 1300°C and the field from 10 to 1000 V/cm; still, the power density for the onset of the flash remains within this same narrow range.

This "universal behavior" shows the significance of power dissipation, and therefore of Joule heating in this phenomenon. However, it is not clear whether or not Joule heating, by itself, is enough to precipitate the extreme nonlinearity of the flash event.

The role of Joule heating is analyzed in terms of the competition between the expenditure of electrical power and blackbody radiation. The result, drawn in nondimensional parameters, given by Eq. (15), shows that the difference between these two quantities varies as the temperature rises. It can remain positive, meaning that Joule heating will continue to produce temperature rise, or it can become negative, a condition which is physically inadmissible since it implies that the heat loss by blackbody radiation exceeds the electrically generated heat within the specimen. Comparison with several data, from 3YSZ, 8YSZ, MgO-doped alumina and composites of alumina, and 3YSZ, show that in many instances of flash sintering the difference between electrical power and blackbody radiation loss is negative, implying that thermal runaway cannot be sustained.

Acknowledgment

This research was supported by a Grant from the Basic Energy Sciences Division of the Department of Energy under grant no. DE-FG02-07ER46403. The author is grateful to Dr. Jean-Marie Lebrun for the analysis given in Fig. 9.

Addendum

Since writing this article the author has noted that the values for PW^* given in Table I are overestimated since they lie above the extrapolation of the Arrhenius line, although Eq. (3) requires it to lie on this line. However, this difference would cause the plots in Figs 4, 5 and 6 to move downwards because the intercept on the y-axis which is equal to R^*, is proportional directly to P_W^*, as in Eq. (17). This correction would place the curves shown in Figs 6, 7 and 8, further down in the negative territory, which is prohibited territory.

References

[1]M. Cologna, B. Rashkova, and R. Raj, "Flash Sintering of Nanograin Zirconia in <5 s at 850°C," *J. Am. Ceram. Soc.*, **93** [11] 3556–9 (2010).
[2]A. L. Prette, M. Cologna, V. Sglavo, and R. Raj, "Flash-Sintering of Co_2MnO_4 Spinel for Solid Oxide Fuel Cell Applications," *J. Power Sources*, **196** [4] 2061–5 (2011).
[3]M. Cologna, A. L. Prette, and R. Raj, "Flash-Sintering of Cubic Yttria-Stabilized Zirconia at 750° C for Possible Use in SOFC Manufacturing," *J. Am. Ceram. Soc.*, **94** [2] 316–9 (2011).
[4]J. C. M'Peko, J. S. Francis, and R. Raj, "Impedance Spectroscopy and Dielectric Properties of Flash Versus Conventionally Sintered Yttria-Doped Zirconia Electroceramics Viewed at the Microstructural Level," *J. Am. Ceram. Soc.*, **96** [12] 3760–7 (2013).
[5]S. K. Jha and R. Raj, "The Effect of Electric Field on Sintering and Electrical Conductivity of Titania," *J. Am. Ceram. Soc.*, **97** [2] 527–34 (2014).
[6]A. Karakuscu, et al., "Defect Structure of Flash-Sintered Strontium Titanate," *J. Am. Ceram. Soc.*, **95** [8] 2531–6 (2012).
[7]M. Cologna, J. S. Francis, and R. Raj, "Field Assisted and Flash Sintering of Alumina and Its Relationship to Conductivity and MgO-Doping," *J. Eur. Ceram. Soc.*, **31** [15] 2827–37 (2011).
[8]H. Yoshida, Y. Sakka, T. Yamamoto, J. M. Lebrun, and R. Raj, "Densification Behaviour and Microstructural Development in Undoped Yttria Prepared by Flash-Sintering," *J. Eur. Ceram. Soc.*, **34** [4] 991–1000 (2014).
[9]J. C. M'Peko, J. S. Francis, and R. Raj, "Field-Assisted Sintering of un-Doped $BaTiO_3$: Microstructure Evolution and Dielectric Permittivity," *J. Eur. Ceram. Soc.*, **34** [15] 3655–60 (2014).
[10]E. Zapata-Solvas, S. Bonilla, P. R. Wilshaw, and R. I. Todd, "Preliminary Investigation of Flash Sintering of SiC," *J. Eur. Ceram. Soc.*, **33** [13] 2811–6 (2013).
[11]K. S. Naik, V. M. Sglavo, and R. Raj, "Field Assisted Sintering of Ceramic Constituted by Alumina and Yttria Stabilized Zirconia," *J. Eur. Ceram. Soc.*, **34** [10] 2435–42 (2014).
[12]J. Wang and R. Raj, "Estimate of the Activation Energies for Boundary Diffusion from Rate-Controlled Sintering of Pure Alumina, and Alumina Doped with Zirconia or Titania," *J. Am. Ceram. Soc.*, **73** [5] 1172–5 (1990).
[13]R. I. Todd, E. Zapata-Solvas, R. S. Bonilla, T. Sneddon, and P. R. Wilshaw, "Electrical Characteristics of Flash Sintering: Thermal Runaway of Joule Heating?" *J. Eur. Ceram. Soc.*, **35** [6] 1865–77 (2015).
[14]Y. Dong and I. Chen, "Predicting the Onset of Flash Sintering," *J. Am. Ceram. Soc.*, **98** [8], 2333–5 (2015).
[15]K. Terauds, et al., "Electroluminescence and the Measurement of Temperature During Stage III of Flash Sintering Experiments," *J. Eur. Ceram. Soc.*, **35** [11] 3195–9 (2015).
[16]J. M. Lebrun, T. G. Morrissey, J. S. Francis, K. C. Seymour, W. M. Kriven, and R. Raj, "Emergence and Extinction of a New Phase During On–Off Experiments Related to Flash Sintering of 3YSZ," *J. Am. Ceram. Soc.*, **98** [5], 1493–7 (2015).
[17]R. Raj, "Joule Heating During Flash-Sintering," *J. Eur. Ceram. Soc.*, **32** [10] 2293–301 (2012).
[18]J. S. Francis, and R. Raj, "Influence of the Field and the Current Limit on Flash Sintering at Isothermal Furnace Temperatures," *J. Am. Ceram. Soc.*, **96** [9] 2754–8 (2013). □